DIRECT NUMERICAL SIMULATIONS OF THE ROD-ROUGHENED TURBULENT BOUNDARY LAYER UNDER PRESSURE GRADIENT

Yi Li
Department of Engineering Mechanics
Tsinghua University
Beijing, China
y-li23@mails.tsinghua.edu.cn

Wei-Xi Huang
Department of Engineering Mechanics
Tsinghua University
Beijing, China
hwx@tsinghua.edu.cn

Chun-Xiao Xu
Department of Engineering Mechanics
Tsinghua University
Beijing, China
xucx@mail.tsinghua.edu.cn

ABSTRACT

Direct numerical simulations of rod-roughened turbulent boundary layers under adverse, zero, and favourable pressure gradients (APG, ZPG, and FPG) were conducted. A modified equivalent boundary layer model was employed to generate the inflow turbulence, facilitating a rapid transition to an equilibrium flow state. Compared to ZPG, APG accelerates boundary layer growth and strengthens the mean velocity wake but suppresses the roughness function. Conversely, FPG decelerates layer growth, weakens the wake, and enhances the roughness function. For the outer-layer velocity defect, the velocity scale ($U_e\delta^*/\delta$) optimally collapses the ZPG and FPG profiles, whereas the free-stream velocity (U_e) is the most robust scaling for APG, under which the mixed scale $\sqrt{U_e u_\tau}$ completely fails. Dynamically, APG amplifies overall turbulence intensities and induces a global secondary outer peak in the spatially averaged streamwise Reynolds stress; in contrast, this peak remains strictly localised above roughness crests in ZPG and FPG flows. Finally, two-point correlations reveal that FPG elongates streamwise vortices and reduces their inclination angles, with APG exerting the exact opposite effect.

INTRODUCTION

Rough-wall turbulent boundary layers (TBLs) with non-zero pressure gradients are common and significant in engineering applications, such as flows over rough aerofoils and turbine blades. Clauser (1954) proposed the pressure gradient parameter, $\beta = (\delta^*/\tau_w)(\mathrm{d}P_e/\mathrm{d}x)$, where δ^* is the displacement thickness, τ_w is the wall shear stress and $\mathrm{d}P_e/\mathrm{d}x$ is the far-field streamwise pressure gradient. If $\beta > 0$, the TBL is subject to APG effects, whereas if $\beta < 0$, it is exposed to the influence of FPG. The TBL is called in an equilibrium state if β is a constant independent of streamwise position.

Existing studies on rough-wall TBLs with pressure gradient (PG) are predominantly experimental. For example, Tay et al. (2009) measured flows over ribs in an asymmetric expanding channel, finding that the combined effect of APG and roughness on thickness growth exceeded individual contributions. Additionally, they observed that the boundary layer thickness of rough TBLs increases less than that of smooth TBLs when the APG increases. They also showed that the combined increase in turbulence intensity and Reynolds shear stress from APG and roughness is greater than their respective effects. Building on these findings, Volino & Schultz (2023) found that rough and smooth walls remain similar in the outer layer under FPG/ZPG but differ under APG. Further, Ghanadi & Djenidi (2022) observed a lack of collapse in the velocity profiles across different pressure gradients. Their spectral and proper orthogonal decomposition (POD) analyses revealed that the pressure gradient predominantly modulates large-scale motions, whereas surface roughness dictates near-wall flow dynamics. Despite these insights, experiments still face challenges in obtaining certain physical quantities, such as turbulent fluctuations of pressure and spanwise velocity.

Numerical simulations of rough TBLs with PG remain limited. The only work in this area is by Yuan & Piomelli (2014, 2015), who studied a flat-plate TBL over roughness with both equilibrium and non-equilibrium FPG. They proposed that the coupled effects of acceleration and roughness increase the mean strain rate. This, in turn, impacts turbulence mainly through higher production and greater wake intensity, subsequently leading to higher pressure drag and intensified energy transfer between the wake and the turbulence. Nevertheless, simulating equilibrium rough TBLs under APG, which would eliminate the history effect, remains a challenge.

Compared to the existing studies, the present direct numerical simulations of rough TBLs with PG solved two main issues: how to acquire accurate quantities which are unavailable for experiments and how to obtain the equilibrium rough TBLs with PG.

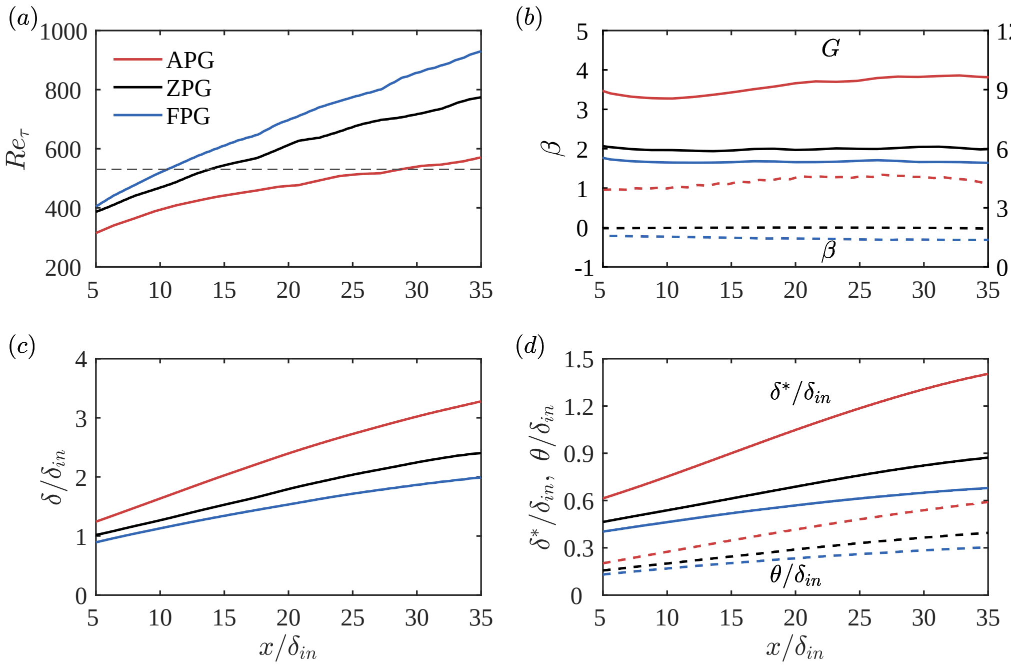

Figure 1. Streamwise variation of (a) Re_τ; (b) shape factor G and pressure gradient parameter β; (c) δ/δ_{in}; (d) $\delta^*/\delta_{in}, \theta/\delta_{in}$.

METHODS

The governing equations of the turbulent boundary layers are as follows.

$$\frac{\partial \boldsymbol{u}}{\partial t} + (\boldsymbol{u}\cdot\nabla)\boldsymbol{u} = -\frac{1}{\rho}\nabla p + \nu\nabla^2\boldsymbol{u} + \boldsymbol{f} \qquad (1)$$

$$\nabla\cdot\boldsymbol{u} = 0 \qquad (2)$$

where $\boldsymbol{u}$ is the velocity vector, p is the pressure, $\boldsymbol{f}$ is momentum forcing, ρ and ν are the density and kinematic viscosity of the fluid. $\boldsymbol{f}$ is calculated by the immersed boundary method used by Huang & Sung (2007) to satisfy the desired no-slip condition at the rough surfaces. The roughness elements are configured as two-dimensional spanwise rods with a height of $k = 0.2\delta_{in}$ and a spacing of $8k$. The pressure gradient is imposed via spatially varying freestream velocity $U_e \sim x^m$, for APG $m = -0.15$ and for FPG $m = 0.25$. The inlet boundary condition combines the mean velocity from a half-channel simulation and the generated turbulence from a modified equivalent boundary layer model proposed by Li et al. (2025). At the outlet, the convective boundary condition $\partial\boldsymbol{u}/\partial t + C\partial\boldsymbol{u}/\partial x = C\partial\boldsymbol{U}_e^o/\partial x$ is imposed, where C is the convection speed and $\boldsymbol{U}_e^o$ is the freestream velocity at the outlet.

The direct numerical simulations used the second-order central difference scheme and the Crank-Nicolson scheme for spatial and temporal discretisation, respectively, which has been validated by Kim et al. (2002). The computational domain is $40\delta_{in}\times 8\delta_{in}\times 8\delta_{in}$ and the grids are $4000\times 256\times 250$ with $Re_{in} = 3500$.

RESULTS

Figure 1 (a) illustrates the streamwise variation of the friction Reynolds number ($Re_\tau = u_\tau\delta/\nu$) for rough-wall boundary layers under APG, ZPG, and FPG conditions with similar inlet friction Reynolds numbers. Here, $u_\tau = (\tau_w/\rho)^{0.5}$ and τ_w is the total drag, which is the sum of the skin-frictional and form drags. The friction Reynolds number exhibits the slowest streamwise growth under APG and the fastest under FPG. The similar effect of APG has been reported by Kitsios et al. (2017) in smooth-wall boundary layers.

Clauser (1954) proposed that both β and the shape factor $G = (H-1)/(H\sqrt{C_f/2})$ being constant is the requirements of self-similar boundary layers. Here $H = \delta^*/\theta$ and $C_f = 2U_e^2/u_\tau^2$. As shown in Figure 1 (b), the pressure gradient parameter β and the shape factor G of three cases remain nearly constant after $x/\delta_{in} = 20$. For APG TBL $\beta = 1.3$ and for FPG TBL $\beta = -0.3$. The gentle variation of β and G throughout the entire computational region ensures equilibrium TBLs and avoids the history effect of pressure gradients.

Figure 1 (c) and (d) present that the APG accelerates the streamwise increase of boundary layer thickness δ and displacement thickness δ^*, momentum thickness θ, and FPG decelerates it. This aligns with the experiments of Ghanadi & Djenidi (2022).

Figure 2 shows the spatially and temporally averaged streamwise velocity over a single roughness pitch at $Re_\tau = 530$, whose streamwise locations are indicated in figure 1 (a) by the horizontal dashed line. The dashed lines in figure 2 is

$$U^+(y) = 1/\kappa\ln(y-d)^+ + B - \Delta U^+, \qquad (3)$$

where $\kappa = 0.41$ and $B = 5.1$ are the smooth-wall constants. Here, d denotes the zero-plane displacement from the physical bottom of the roughness ($y = 0$) to the virtual origin, determined by maximising the quality of the logarithmic fit. Additionally, ΔU^+ is the roughness

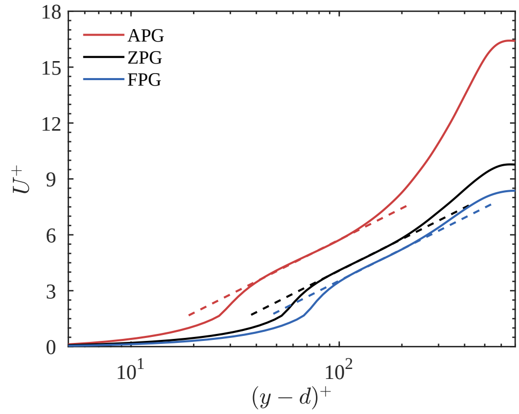

Figure 2. Profiles of inner-scaled mean streamwise velocity U^+ at $Re_\tau = 530$. Dashed lines denote the logarithmic law $U^+(y) = 1/\kappa \ln(y-d)^+ + B - \Delta U^+$.

function, representing the downward velocity shift from the smooth-wall logarithmic law. In the present study, $d = 0.29k$ for all three cases. The roughness function evaluates to $\Delta U^+ = 10.6$, 12.3, and 12.8 for the APG, ZPG, and FPG conditions, respectively. This increasing trend indicates that the FPG effectively enhances the wall roughness, a finding consistent with the results of Volino & Schultz (2023). The wake region is strengthened in the APG case and weakened in the FPG case, which is consistent with the effect of pressure gradient in the smooth boundary layers of Harun et al. (2013).

As illustrated in figure 1 (b), the flows have reached the equilibrium state. Therefore, we seek an appropriate outer scaling that enables the spanwise and temporal averaged velocity defect profiles at various streamwise positions to collapse onto a single curve, as shown in figure 3. Given that the velocity within the roughness sublayer is severely influenced by the rough surface, our scaling is restricted to the outer region with $y > 0.2\delta$. In figure 3, y is normalized by the outer length scale δ and the mean velocity defect is normalized using the ZS velocity scale $U_e\delta^*/\delta$ proposed by Zagarola & Smits (1998), the mixed inner-outer scale $\sqrt{u_\tau U_e}$ proposed by DrGraaff & Eaton (2000), and the free-stream velocity (U_e), respectively. Previously, the velocity scale $U_e\delta^*/\delta$ has been employed to scale the mean velocity of APG turbulent boundary layers such as Maciel et al. (2018); Pozuelo et al. (2022). The mixed velocity scale is utilized for rough ZPG boundary layers such as Jiménez (2004). As depicted by the gray-black lines in figure 3 (a), the outer-region velocity defect profiles of the rough ZPG boundary layer at different streamwise locations collapse almost perfectly into a single solid line when scaled by $U_e\delta^*/\delta$. Furthermore, this scale is equally applicable to rough FPG boundary layers. However, for rough APG boundary layers, the free-stream velocity yields the best scaling performance, outperforming the $U_e\delta^*/\delta$, while the mixed velocity scale completely fails under rough APG conditions.

Figure 4 (a) presents the Reynolds stress profiles spatially averaged over a single roughness pitch. At an equivalent friction Reynolds number, the magnitudes of the Reynolds stresses under APG are significantly higher than those in the FPG and ZPG cases, indicating a substantial enhancement of turbulence intensity.

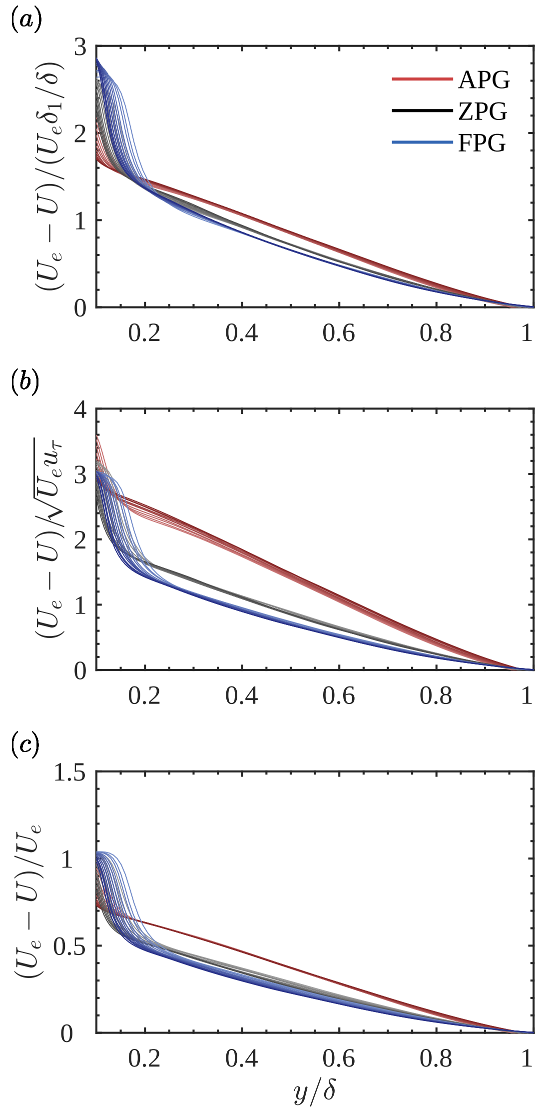

Figure 3. Velocity defect profiles with different scalings: (a) $(U_e-U)/(U_e\delta^*/\delta)$; (b) $(U_e-U)/\sqrt{U_e u_\tau}$; (c) $(U_e-U)/U_e$. Lighter to darker colours indicate the streamwise locations from upstream to downstream.

Furthermore, the $\langle u'u' \rangle^+$ profile for the APG case exhibits a secondary peak in the outer region that exceeds the inner-layer peak, demonstrating the intensification of large-scale energy. This observation is consistent with the findings of Monty et al. (2011) and Lee (2017) regarding smooth-wall APG boundary layers.

Notably, as shown in figure 4 (b), above the centre of the roughness crest, a secondary outer peak emerges for all three cases (APG, ZPG, and FPG). Due to the roughness crest, the bypass flow induces strong mean velocity shear, leading to a localised increase in the streamwise Reynolds stress. This is not contradictory to the streamwise averaged results in figure 4 (a); for the ZPG and FPG cases, the outer $\langle u'u' \rangle^+$ peak exists only within the immediate vicinity of the roughness crest. Consequently, these localised peaks are smoothed out during the spatial averaging process across the roughness pitch,

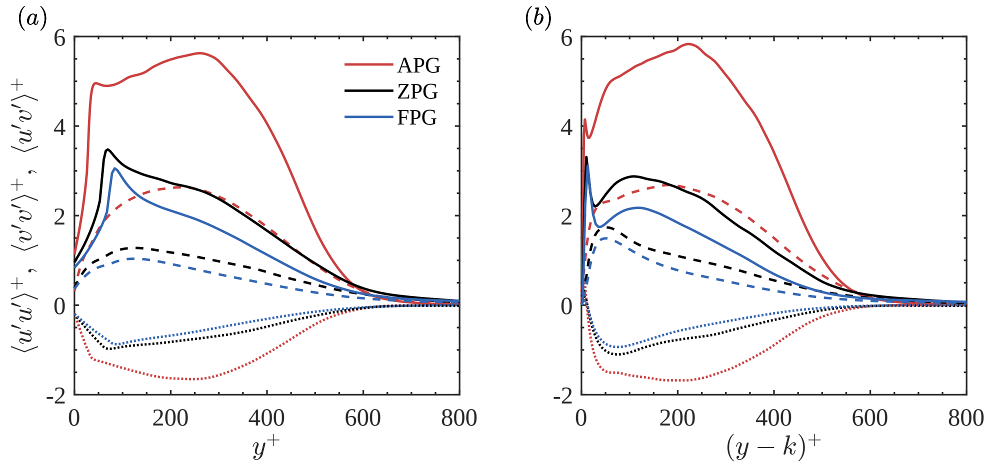

Figure 4. Profiles of the Reynolds stresses $\langle u'u' \rangle^+$ (solid lines), $\langle v'v' \rangle^+$ (dashed lines), and $\langle u'v' \rangle^+$ (dotted lines) at $Re_\tau = 530$: (a) spatially averaged over a single roughness pitch; (b) evaluated at the centre of the roughness crest.

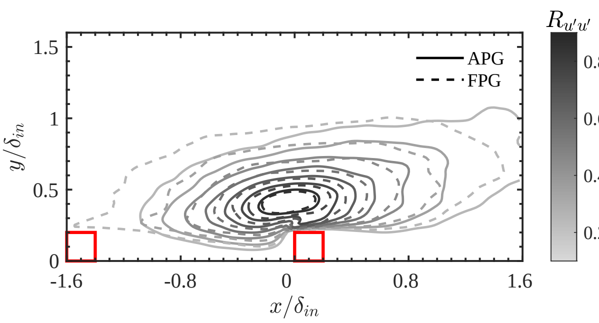

Figure 5. Contours of $R_{u'u'}$ for rough APG and FPG TBLs. The red squares denote the cross-sections of the roughness rods.

resulting in the absence of a distinct outer peak for these two cases in figure 4 (a).

Figure 5 illustrates the two-point correlation of streamwise fluctuating velocity u', defined as

$$R_{u'u'}(x,y) = \frac{\langle u'(x_{ref}, y_{ref}) u'(x,y) \rangle}{\langle u'u' \rangle (x_{ref}, y_{ref})}, \quad (4)$$

where $\langle \cdot \rangle$ denotes averaging over the spanwise direction and time. The wall-normal reference position is fixed at $y_{ref} = 0.4\delta$, characterising the mid-boundary-layer region. The streamwise reference positions, x_{ref}, are located at the leading edges of the 6th and 17th roughness rods for the FPG and APG cases, respectively. At these stations, both boundary layers share a matched friction Reynolds number of $Re_\tau \approx 530$. The contours of the two-point correlation are representative of hairpin vortex structures as illustrated by Volino & Schultz (2023). In the present study, the inclination angle of the contours for the APG case is slightly steeper than that for the FPG case. This indicates that even under pronounced roughness conditions ($k_s^+ \approx 310$ for FPG and $k_s^+ \approx 760$ for APG), the applied pressure gradient continues to modulate the near-wall flow structures.

CONCLUSIONS

Direct numerical simulations of turbulent boundary layers over two-dimensional spanwise roughness rods were performed to investigate the coupled effects of surface roughness and pressure gradients (APG, ZPG, and FPG). Strictly equilibrium states (constant β and G) were achieved, isolating pressure gradient effects from upstream historical influence. Key findings include:

Regarding the mean flow, FPG enhances the roughness function, while APG strengthens the wake. For the outer-layer velocity defect, the Zagarola–Smits scale optimally collapses ZPG and FPG profiles, whereas the free-stream velocity (U_e) is the most robust scaling for the APG condition. Furthermore, APG amplifies overall turbulence, generating a global secondary outer peak in the spatially averaged streamwise Reynolds stress ($\langle u'u' \rangle^+$). Conversely, this peak is purely localised above roughness crests in ZPG and FPG flows. Structurally, two-point correlations reveal that APG steepens the inclination of hairpin vortices relative to FPG. Ultimately, these results demonstrate that despite severe roughness, pressure gradients actively modulate near-wall topology, offering new scaling and structural insights that are challenging to achieve experimentally.

REFERENCES

Clauser, Francis H. 1954 Turbulent boundary layers in adverse pressure gradients. Journal of the Aeronautical Sciences 21 (2), 91–108.

DrGraaff, DAVID B. & Eaton, JOHN K. 2000 Reynolds-number scaling of the flat-plate turbulent boundary layer. Journal of Fluid Mechanics 422, 319–346.

Ghanadi, F. & Djenidi, L. 2022 Study of a rough-wall turbulent boundary layer under pressure gradient. Journal of Fluid Mechanics 938, A17.

Harun, Zambri, Monty, Jason P., Mathis, Romain & Marusic, Ivan 2013 Pressure gradient effects on the large-scale structure of turbulent boundary layers. Journal of Fluid Mechanics 715, 477–498.

Huang, Wei-Xi & Sung, Hyung Jin 2007 Improvement of mass source/sink for an immersed boundary method. International Journal for Numerical Methods in Fluids 53 (11), 1659–1671.

Jiménez, Javier 2004 Turbulent flows over rough walls. Annual Review of Fluid Mechanics 36 (1), 173–196.

Kim, Kyoungyoun, Baek, Seung-Jin & Sung, Hyung Jin 2002 An implicit velocity decoupling procedure for the incompressible navier–stokes equations. International journal for numerical methods in fluids 38 (2), 125–138.

Kitsios, V., Sekimoto, A., Atkinson, C., Sillero, J. A., Borrell, G., Gungor, A. G., Jiménez, J. & Soria, J. 2017 Direct numerical simulation of a self-similar adverse pressure gradient turbulent boundary layer at the verge of separation. Journal of Fluid Mechanics 829, 392–419.

Lee, Jae Hwa 2017 Large-scale motions in turbulent boundary layers subjected to adverse pressure gradients. Journal of Fluid Mechanics 810, 323–361.

Li, Yi, Shu, Zheng-Qin, Huang, Wei-Xi & Xu, Chun-Xiao 2025 Inflow turbulence generation for turbulent boundary layer with adverse pressure gradient using an equivalent boundary layer model. Physics of Fluids 37 (10), 105143.

Maciel, Yvan, Wei, Tie, Gungor, Ayse G. & Simens, Mark P. 2018 Outer scales and parameters of adverse-pressure-gradient turbulent boundary layers. Journal of Fluid Mechanics 844, 5–35.

Monty, J.P., Harun, Z. & Marusic, I. 2011 A parametric study of adverse pressure gradient turbulent boundary layers. International Journal of Heat and Fluid Flow 32 (3), 575–585.

Pozuelo, Ramón, Li, Qiang, Schlatter, Philipp & Vinuesa, Ricardo 2022 An adverse-pressure-gradient turbulent boundary layer with nearly constant $\beta \simeq 1.4$ up to $re_\theta \simeq 8700$. Journal of Fluid Mechanics 939, A34.

Tay, G.F.K., Kuhn, D.C.S. & Tachie, M.F. 2009 Influence of adverse pressure gradient on rough-wall turbulent flows. International Journal of Heat and Fluid Flow 30 (2), 249–265.

Volino, Ralph J. & Schultz, Michael P. 2023 Comparison of smooth- and rough-wall non-equilibrium boundary layers with favourable and adverse pressure gradients. Journal of Fluid Mechanics 959, A35.

Yuan, J. & Piomelli, U. 2014 Numerical simulations of sink-flow boundary layers over rough surfaces. Physics of Fluids 26 (1), 015113.

Yuan, J. & Piomelli, U. 2015 Numerical simulation of a spatially developing accelerating boundary layer over roughness. Journal of Fluid Mechanics 780, 192–214.

Zagarola, Mark V. & Smits, Alexander J. 1998 Mean-flow scaling of turbulent pipe flow. Journal of Fluid Mechanics 373, 33–79.